

***A Himalayan-Scale Orogen in the Central African Copperbelt and the Formation of a World-Class Metal Province.***

Tobermory Mackay-Champion<sup>1,2</sup>

<sup>1</sup>University of Oxford, UK. <sup>2</sup>University of Bristol, UK.

tmackaychampion@gmail.com

This paper is a non-peer reviewed preprint submitted to EarthArXiv. The paper has been submitted to Science Advances for peer review.

# 2 A Himalayan-Scale Orogen in the Central African 3 Copperbelt and the Formation of a World-Class Metal 4 Province.

5 **Tobermory Mackay-Champion**  \*1

6 <sup>1</sup>Department of Earth Sciences, University of Oxford, South Parks Road, Oxford, UK.

7 **Abstract** The Central African Copperbelt (CACB) of Zambia and the Democratic Republic of the  
8 Congo is the world's largest sediment-hosted copper-cobalt province. It comprises Tonian–Ediacaran  
9 sedimentary rocks of the Katangan Basin and Ediacaran–Cambrian metamorphic and intrusive  
10 rocks formed during the assembly of Gondwana. The age distribution of metal deposits within  
11 the CACB peaks during the orogeny, indicating a significant orogenic control on mineralization.  
12 This study synthesizes existing structural, petrological, geochronological, and geophysical data to  
13 propose a new geodynamic model that reinterprets the CACB as a Himalayan-scale, continental-  
14 collision orogenic system. Its tectonic evolution is characteristic of a typical Wilson Cycle: conti-  
15 nental rifting and ocean basin formation (~880–650 Ma); oceanic subduction and pre-collisional  
16 metamorphism ( $\leq 650$  Ma); continent-continent collision ( $\leq 570$  Ma), leading to significant crustal  
17 thickening with burial depths reaching up to 45 km (~530 Ma); and late-stage thrusting and mag-  
18 matism ( $\leq 510$  Ma). The new model indicates that the CACB benefitted from two principal metal  
19 sources: metals derived from basement erosion, and metals introduced by magmatism during and  
20 after continent–continent collision, which is newly identified in this study. The next generation of  
21 metal deposits in the CACB will be found by locating outcropping or shallow subsurface magmatic  
22 intrusions.

## 23 1 Introduction

24 Sediment-hosted copper (Cu) deposits—comprising disseminated and veinlet Cu-sulfides within sedimentary rocks—  
25 currently account for ~23 % of global copper production (Hammarstrom et al., 2019). These deposits are particularly  
26 attractive due to their relatively high grades and substantial ore volumes compared to porphyry Cu and volcanogenic  
27 massive sulfide (VMS) deposits, respectively (Dominish et al., 2019). However, exploration for sediment-hosted metal  
28 deposits has generally been less successful than for magmatic systems, largely due to an incomplete understanding  
29 of the first-order tectonic controls governing their distribution (Hoggard et al., 2020).

30 This challenge is exemplified by the Central African Copperbelt (CACB) of Zambia and the Democratic Republic  
31 of the Congo. The CACB is the world's largest sediment-hosted copper and cobalt province and contributes ~14 %

\*Corresponding author: tmackaychampion@gmail.com

and ~60 % of the world's supply of these two metals, respectively (Selley et al., 2005). The CACB comprises Tonian–Ediacaran sedimentary rocks of the Katangan Basin and Ediacaran–Cambrian metamorphic and intrusive rocks. These rock assemblages formed through a sequence of continental rifting followed by basin closure and continent–continent collision between the Congo and Kalahari Cratons during the assembly of Gondwana (Porada and Berhorst, 2000). Research efforts have primarily focused on constraining the extensional history of the Katangan Basin, often under the assumption that mineralization is predominantly syn-diagenetic (Hitzman and Broughton, 2017). However, the age distribution of metal deposits peaks during the assembly of Gondwana, indicating a significant orogenic control on mineralization (Sillitoe et al., 2017). Despite this, no detailed geodynamic model exists for the CACB during this period. Interpretations of the CACB have largely emphasized a sedimentary-basin framework, with comparatively little focus on its orogenic evolution. Without this whole-system perspective, fundamental controls on the mineral system—including thermal gradients, fluid pathways, source rocks, metal traps, and crustal architecture—remain poorly understood. The CACB is estimated to contain ~170 Mt of undiscovered copper resources (Hammarstrom et al., 2019), but exploration is significantly hampered by this knowledge gap (McCuaig and Hronsky, 2014).

In this study, I present a meta-analysis of existing structural, petrological, geochronological, and geophysical data to develop a new geodynamic model for the evolution of the CACB. I demonstrate that the CACB can be more accurately understood within an orogenic framework rather than through the traditional sedimentary-basin perspective. It exhibits striking similarities to classic collisional orogenic belts such as the Himalaya-Karakoram and the Scottish Caledonides, including regional metamorphism up to kyanite-grade conditions as well as a comparable tectonic configuration. The new model also offers an improved understanding of the mineral systems governing the CACB, particularly highlighting the potential role of magmatism-driven mineralization. In Section 2, I outline the large-scale tectonic setting of the CACB. Section 3 presents a reinterpretation of the geological characteristics of individual domains within the CACB orogenic system, revealing a previously unrecognised tectonic framework. The new geodynamic model is introduced in Section 4, followed in Section 5 by an analysis of the CACB mineral system within this new framework. Despite differences in erosion levels among orogens of varying ages, there are clear similarities in their overall structural architecture, metamorphic conditions, and geochronological evolution (Weller et al., 2021). Accordingly, comparisons with analogous orogenic systems are drawn where relevant to enhance understanding of the CACB.

## 2 Geological setting of the CACB

The geological evolution of the CACB and its surrounding regions can be broadly categorized into four major time periods and associated litho-tectonic assemblages (Figure 1): (1) the Archaean and Palaeoproterozoic Congo, Bangweulu, and Kalahari cratons, which crop out to the northwest, northeast, and south of the CACB respectively. These terranes exhibit lithospheric thicknesses in excess of 200 km (Schaeffer and Lebedev, 2013). (2) the Mesoproterozoic Irumide and Kibaran belts, which formed part of the Central African Shield during the assembly of Rodinia (Vileneuve et al., 2023), (3) the Katangan Basin, which formed as a result of extension and subsequent rifting between the Congo and Kalahari cratons during the Neoproterozoic (Purkiss, 2025; Daly et al., 2025) and, (4) the < 650 Ma Lufilian Orogen, comprising rocks up to kyanite-grade metamorphic conditions and high levels of deformation (Porada and

68 Berhorst, 2000). The orogen formed as a result of basin closure and orogenesis associated with continent-continent  
69 collision and the assembly of Gondwana. This study uses the term CACB to refer to both the Katangan Basin and the  
70 Lufilian Orogen, reflecting their temporal and structural continuity as well as the presence of metal deposits in both  
71 regions.

### 72 **3 Tectonic domains of the CACB**

73 The CACB can be viewed as an approximately north-to-south progression from the Congo Craton through: (1) the  
74 Katangan Basin, (2) the External Fold-Thrust Belt, (3) the Domes Region, (4) the Synclinorial Belt, (5) the Lufilian  
75 Suture Zone (comprising the Katanga High and Zambezi Belt), and finally the Kalahari Craton (Figure 1). In contrast  
76 to the traditional view, the Katanga High and Zambezi Belt are treated here as a single composite domain based  
77 on their metamorphic, structural, and geochronological continuity (Figure 1; see Section 3.5). The following sub-  
78 sections discuss the structural, metamorphic, and geochronological characteristics of each domain.

#### 79 **3.1 Katangan Basin**

80 This region is characterized by sub-horizontal to gently dipping Katangan Supergroup sedimentary rocks onlapping  
81 Congo, Kibaran, Bangweulu, and Irumide basement rocks (Daly et al., 2025). This represents an autochthonous  
82 remnant of the Katangan Basin, which formed as a result of two-stage rifting between the Congo craton to the north  
83 and the Kalahari craton to the south (present day coordinates) over a protracted ~300 Myr timeframe (Purkiss, 2025;  
84 Daly et al., 2025): The first stage of rifting began sometime after ~880 Ma during the Tonian Period, resulting in the  
85 deposition of syn-rift Lower Roan Group sedimentary rocks. Above it, the Upper Roan Group marks a transition  
86 to post-rift conditions, representing shallow marine and coastal environments formed during thermal subsidence.  
87 The Mwashia Group reflects a second period of rifting and associated magmatic activity commencing at ~765 Ma,  
88 with deepening of the basin characterised by marine flooding surfaces (Purkiss, 2025). The northwest and southeast  
89 margins of the basin comprise fault-controlled subbasins with extensive Mwashia-age extrusive and intrusive mafic  
90 units (Kampunzu et al., 2000). Above the Mwashia lies the Nguba Group, which spans the Sturtian glaciation and  
91 represents a deep, often sediment-restricted basin bounded by a maximum flooding surface. Finally, the Kundelungu  
92 Group was deposited from the beginning of the Ediacaran period and represents a distal, quiet basin (Purkiss, 2025).  
93 This culminates in the Plateau Group, interpreted as a continental molasse (Wendorff, 2005). Historically referred to  
94 as the Shaba, Katangan or Kundelungu aulacogen or Golfe du Katanga (De Swardt et al., 1964; Porada and Berhorst,  
95 2000), this northern region has previously been recognized as the stable foreland of the CACB (e.g., Wendorff, 2005).  
96 The hydrothermal, vein-hosted copper deposits of Dikulushi, Safari, and Shaba are found here (Taylor et al., 2013;  
97 Padilla et al., 2021).

#### 98 **3.2 External Fold-Thrust Belt**

99 Structurally above the foreland succession lies the External Fold-Thrust Belt, which crops out along the Zambia-  
100 DRC border and the southern DRC. This domain contains the highest number of known metal deposits, including  
101 mines such as Konkola with reserves of  $\geq 140.3$  Mt Cu. The belt is characterized by northward-directed thin-skinned  
102 thrusting and imbrication of Katangan Supergroup sedimentary rocks and their low-grade metamorphic equivalents

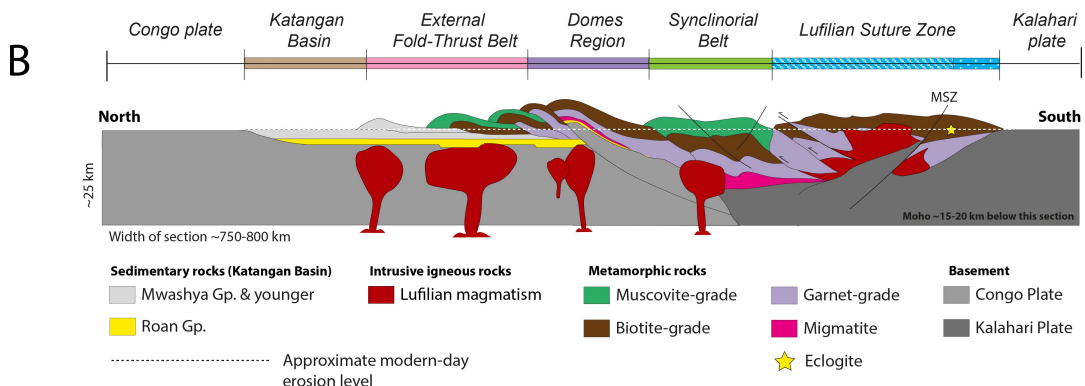
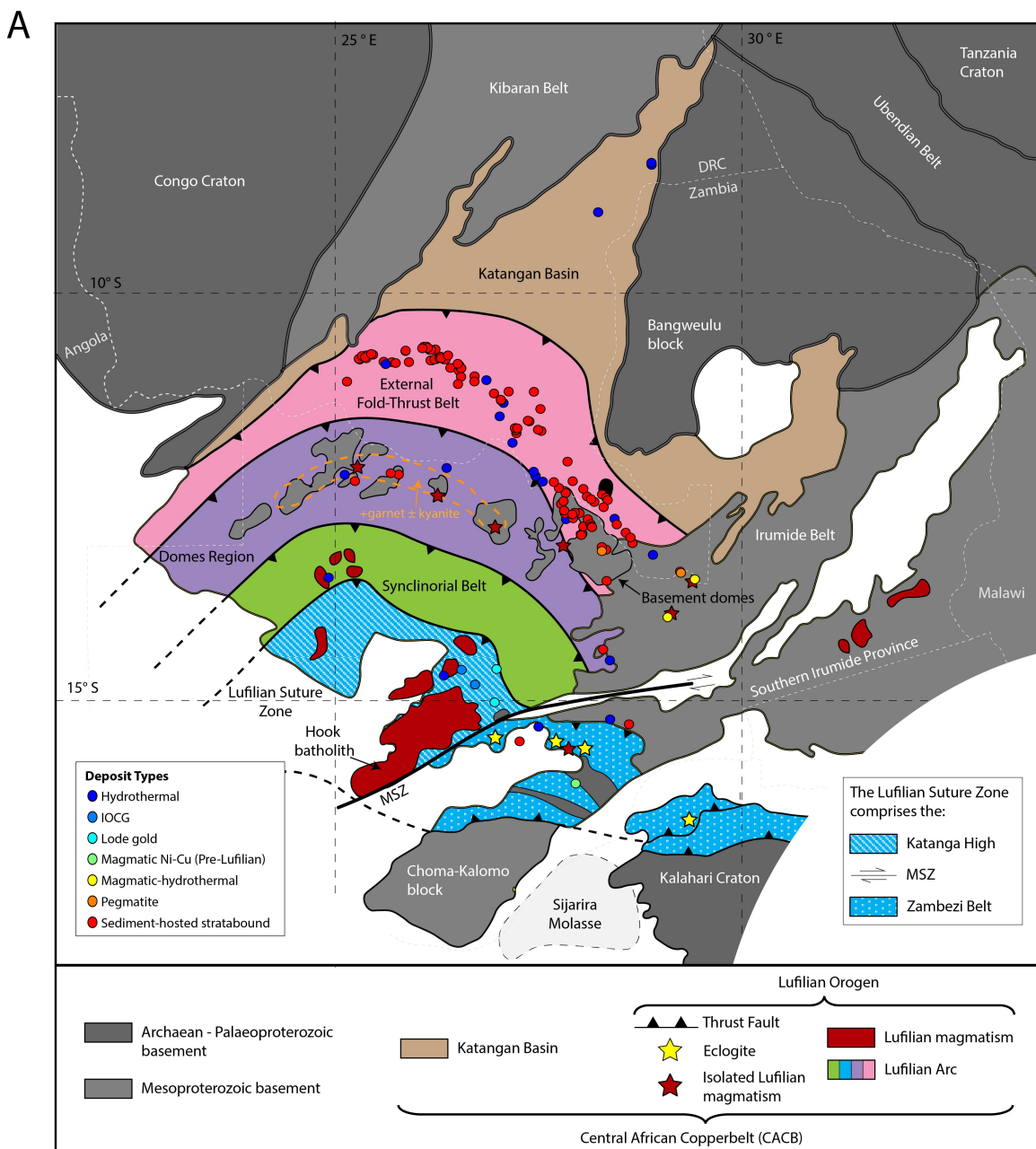


**Figure 1** A) Tectonic map of the Central African Copperbelt modified after Eglinger et al. (2013) and Daly et al. (2025). The newly defined *Lufilian Suture Zone* has been divided into the north-western Katanga High and the south-eastern Zambezi Belt, separated by the Mwembeshi Shear Zone (MSZ). These terranes are combined due to their metamorphic, structural, and igneous continuity during the Lufilian orogeny (Section 3.5). The mine locations and deposit types are taken from Taylor et al. (2013) and Padilla et al. (2021). B) Schematic cross-section of the Central African Copperbelt. N.B. the Lufilian magmatism is not to scale.

103 above evaporite-rich detachments (Coward and Daly, 1984). These detachments accommodated significant lateral  
104 transport of up to 65–150 km northwards (Porada and Berhorst, 2000; Jackson et al., 2003). The evaporites also facil-  
105 itated fluid overpressuring and diapirism, as well as the extrusion of salt glaciers (Jackson et al., 2003). The metamor-  
106 phic grade of the external belt decreases from greenschist to prehnite-pumpellyite down structural section towards  
107 the north (Selley et al., 2005). The belt hosts Lufilian-age pegmatites associated with emerald mineralization and  
108 magmatic-hydrothermal deposits aged between 530–517 Ma (Perelló et al., 2022; Seifert et al., 2004). Along strike to  
109 the south-east, the Southern Irumide Belt contains granites and syenites emplaced between 534–465 Ma (Johnson  
110 et al., 2006). These intrusions likely represent magmatic bodies emplaced into the footwall of the External Fold-  
111 Thrust Belt, now exposed as a result of extensive erosion and Cenozoic rifting. These intrusions are coeval with  
112 high-pressure metamorphism in the Chewore-Rufunsa terrane of the Southern Irumide Belt (Johnson et al., 2006).  
113 Metamorphic monazite ages in the fold-thrust belt cluster around 530 Ma, while Ar-Ar biotite cooling ages cluster  
114 between 490–475 Ma (Rainaud et al., 2005) (Figure 3). This reflects peak metamorphism followed by post-tectonic  
115 uplift and cooling.

### 116 3.3 Domes Region

117 Structurally above the fold-thrust belt lies the Domes Region, named after five antiformal domes of Mesoproterozoic  
118 basement rock that crop out along strike from one another in northwest Zambia. The Domes Region is an arcu-  
119 ate zone approximately 50 km across strike and represents the deepest structural levels and highest metamorphic  
120 grades of the entire CACB. Based on these observations, the Domes Region has previously been interpreted as the  
121 locus of maximum shortening during the Katangan Basin inversion (Goscombe et al., 2020; Daly et al., 2025). The  
122 metasedimentary rocks in the Domes Region range from biotite to garnet-kyanite grade, with local evidence for par-  
123 tial melting (Cosi et al., 1992; John et al., 2004; Eglinger et al., 2016). Peak metamorphic pressures of 13 kbar (~45 km  
124 burial) indicate substantial crustal shortening and thickening. These metamorphic rocks can now be found in thrust  
125 contact with undeformed, unmetamorphosed Katangan sedimentary rocks in underlying half-grabens (Daly et al.,  
126 2025). This requires substantial lateral transport from their site of metamorphism—consistent with the large dis-  
127 placements seen in the External Fold-Thrust Belt.

128 Peak metamorphic conditions in the Domes Region were achieved at ~530 Ma (monazite—John et al., 2004; garnet—  
129 Eglinger et al., 2016). The region hosts significant mineralization, including Kansanshi and Sentinel with resources  
130 of 1,125.4 Mt and 648.7 Mt Cu respectively, as well as the Enterprise hydrothermal nickel mine (Capistrant et al., 2015).  
131 The Domes Region also hosts Lufilian-age pegmatites (~ 530 Ma; Selley et al., 2018) and late-Cambrian alkali granites  
132 and nepheline syenites (Cosi et al., 1992). These intrusions likely correspond to granitic bodies inferred beneath the  
133 northern CACB from magnetic anomaly data (Selley et al., 2018). Supporting this interpretation, regional gravity data  
134 indicate that the Domes Region exhibits anomalously low mass, consistent with substantial volumes of low-density  
135 granitic material at depth (Selley et al., 2018).

### 136 3.4 Synclinorial Belt

137 South of the Domes Region lies the Synclinorial Belt, composed of intensely deformed rocks ranging from argilla-  
138 ceous sedimentary rocks to biotite-grade metapelites (Porada and Berhorst, 2000; Goscombe et al., 2020). It features

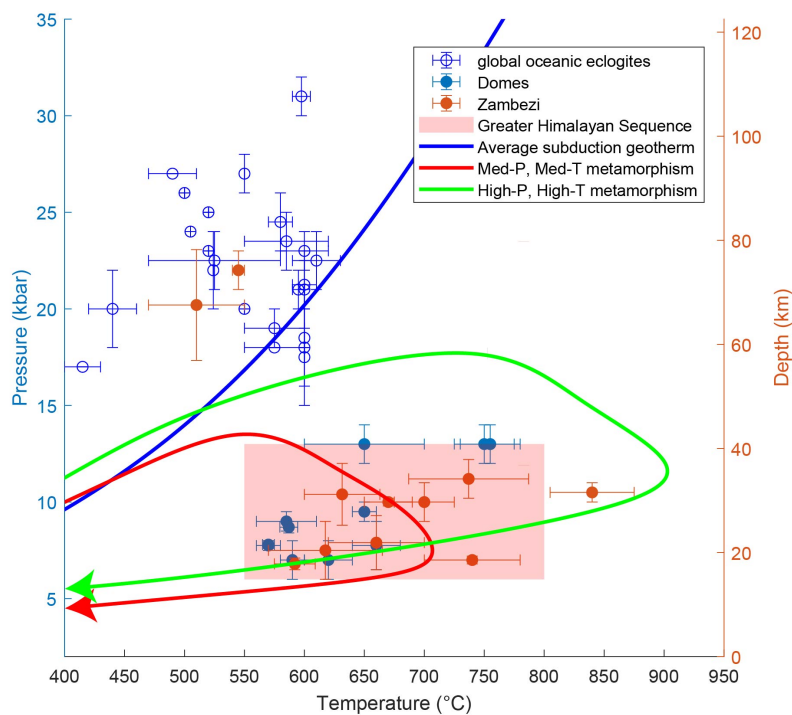


**Figure 2** Pressure-temperature conditions experienced by the Domes Region and Zambezi Belt of the Lufilian Suture Zone. The Greater Himalayan Sequence conditions were taken from [Waters \(2019\)](#). The compilation of global oceanic eclogites from [Chen et al. \(2013\)](#), and the Barrovian P-T paths from [Weller et al. \(2021\)](#). The high pressures recorded in the CACB necessitate significant crustal thickening.

139 steep, north-vergent folds and shows little evidence of salt tectonics ([Daly et al., 2025](#)). This domain remains relatively  
 140 understudied, due to limited outcrop and the lack of active mining operations.

### 141 3.5 Lufilian Suture Zone

142 Structurally overlying the Synclinorial Belt is the newly defined Lufilian Suture Zone, comprising the Katanga High,  
 143 Hook Batholith, Mwembeshi Shear Zone, and Zambezi Belt. This unification of previously distinct lithotectonic as-  
 144 semblages is based on a revised interpretation of the Mwembeshi Shear Zone, outlined below.

#### 145 3.5.1 The Mwembeshi Shear Zone

146 The south-eastern margin of the CACB has typically been defined by the Mwembeshi Shear Zone (MSZ) (e.g., [De](#)  
 147 [Swardt et al., 1964](#)), although its tectonic significance is debated. Some regard the MSZ as a suture zone between  
 148 the Congo and Kalahari cratons (e.g., [Coward and Daly, 1984](#); [Daly et al., 2025](#)). However, no change in shear-wave  
 149 anisotropy or crustal thickness is observed across the MSZ ([Kounoudis et al., 2024](#); [Ogden et al., 2025](#)). Sedimentary  
 150 successions can be traced into the northern part of the Zambezi Belt from the southern Katanga High ([Porada and](#)  
 151 [Berhorst, 2000](#)), and there is a continuity of kyanite-grade metamorphism and structures between the northern part  
 152 of the Zambezi Belt and the Matala Dome, which lie on opposing sides of the MSZ ([Naydenov et al., 2016](#); [Simpson,](#)  
 153 [1962](#)). These observations suggest that the MSZ is not a lithospheric-scale structure contrasting significantly distinct  
 154 geological terranes ([Naydenov et al., 2014](#)). Consequently, the MSZ may be better interpreted as a minimal-offset fault  
 155 that divides the otherwise continuous Katanga High, Hook Batholith, and Zambezi Belt. These regions are therefore  
 156 more appropriately regarded as components of a unified Lufilian Suture Zone.

### 157 3.5.2 The Katanga High and the Hook Batholith

158 The Katanga High comprises extensive outcrops of carbonate rocks and low- to kyanite-grade metapelites, with  
159 north-south-trending folds cross-cut in the north by an east-northeast to west-southwest fold belt (De Swardt et al.,  
160 1964; Naydenov et al., 2016). The region also contains the Matala Dome, a basement inlier surrounded by kyanite-  
161 grade metasedimentary rocks (Naydenov et al., 2016).

162 The south-east section of the Katanga High is intruded by the Hook Batholith, a syn-tectonic, 570–530 Ma, bi-  
163 modal magmatic body (Hanson et al., 1993; Milani et al., 2015; Naydenov et al., 2014). The batholith predominantly  
164 crops out in south-west Zambia, but can also be found in the Zambezi Belt (Hanson et al., 1988). The felsic units  
165 consist of an alkali-calcic suite of monzogranite, granodiorite and granite and an alkali suite of syenite and alkali-  
166 granite (Naydenov et al., 2014). High primary water contents in the Hook Batholith are indicated by the abundance of  
167 primary amphibole (Naydenov et al., 2014). The metaluminous geochemistry and Sr–Nd isotopic signatures, which  
168 overlap with those of ocean-island basalts, rule out derivation from a purely sedimentary protolith and instead point  
169 to significant contributions from mantle-lithologies. This is supported by the presence of syn-tectonic gabbroic in-  
170 trusions (Milani et al., 2015) and underpins the hypothesis that the Hook Batholith began forming above a subducting  
171 slab, where mantle-derived melts intruded and triggered partial melting of the overlying crust (Milani et al., 2015;  
172 Naydenov et al., 2014). The Hook Batholith hosts a number of Cu deposits, some with iron oxide-copper-gold (IOCG)  
173 characteristics (Milani et al., 2019).

### 174 3.5.3 The Zambezi Belt

175 To the southeast of the MSZ lies the Zambezi Belt of southern Zambia and northern Zimbabwe. The Zambezi belt  
176 comprises the Zambezi Supercrustal Sequence (ZSC) and inliers of Mesoproterozoic gneissic and granitoid basement  
177 (Hanson et al., 1988). The ZSC is a sequence of Neoproterozoic sedimentary, volcanic and volcaniclastic rocks that  
178 have been variably metamorphosed up to upper amphibolite-facies conditions (Johnson et al., 2007). The protoliths  
179 of the ZSC are interpreted to be the correlatives of the lower units of the Katangan Supergroup (De Swardt et al.,  
180 1964; Johnson et al., 2007). The Zambezi Belt lies upon a Mesoproterozoic granitic basement including the ~1106 Ma  
181 Mpande Gneiss and the ~1090 Ma Munali Hills Granite (Hanson et al., 1988; Katongo et al., 2004). Extension in the  
182 Zambezi Belt began at ~880 Ma, with the basement unconformably overlain by a series of bimodal metavolcanic  
183 rocks and phyllites known as the Kafue Rhyolite Formation and the Nazingwe Formation, respectively (Hanson et al.,  
184 1993; Johnson et al., 2007). This was coeval with the onset of extension in the Katangan Basin, as constrained by  
185 the  $883 \pm 10$  Ma age of the Nchanga Granite (Armstrong et al., 2005). Continued extension saw the intrusion of the  
186 ~820 Ma Ngoma Gneiss, and other magmatic bodies such as the Munali ultramafic body, which hosts a magmatic  
187 sulfide nickel deposit (Holwell et al., 2017). A second phase of magmatism occurred between 764–737 Ma, preserved  
188 in the Makuti Group felsic extrusives of the Central Zambezi Belt (Dirks et al., 1999), which overlaps with the Mwashia-  
189 age rifting event and accompanying magmatism in the Katangan Basin (Purkiss, 2025).

190 During the assembly of Gondwana, the Zambezi Belt experienced significant NE–SW shortening, developing a  
191 steep, bivergent flower structure that exhumed reworked basement thrust slices and emplaced allochthonous nappes  
192 above the northern margin of the Kalahari Craton (Johnson et al., 2007). The uppermost section of the ZSC hosts

193 numerous peridotitic, gabbroic, and metagabbroic bodies with N-MORB signatures, interpreted as a dismembered  
194 ophiolite sequence (John et al., 2003; Johnson et al., 2005). These bodies occur in close association with eclogites  
195 interpreted to have formed in an oceanic subduction-zone setting. These eclogites are dated between  $659 \pm 14$  Ma  
196 and  $595 \pm 10$  Ma (Vrána et al., 1975; Johnson et al., 2005; John et al., 2003), and record peak prograde conditions of  
197  $540$ – $550$  °C at  $21.0$ – $23.0$  kbar (Chombwa locality) and  $470$ – $550$  °C at  $17.8$ – $23.0$  kbar (Lusaka locality) (Goscombe et al.,  
198 2020). Contemporaneous with eclogite formation, rocks of the Zambezi Belt experienced amphibolite-facies meta-  
199 morphism and monazite growth at  $650$ – $630$  Ma, indicative of metamorphism along the Kalahari Craton margin prior  
200 to continent–continent collision (Sakuwaha et al., 2022). This is followed by a pronounced cluster of metamorphic  
201 monazite ages between  $570$ – $530$  Ma, corresponding to metamorphic conditions of  $10$ – $12$  kbar (Johnson et al., 2005;  
202 Goscombe et al., 2020; Sakuwaha et al., 2022; ?; Kuribara et al., 2019). This is coeval with peak metamorphism in the  
203 Domes Region, with both the Domes Region and the Zambezi Belt attaining comparable peak metamorphic condi-  
204 tions (Figure 2).

### 205 3.6 Southern margin

206 The Kalahari Craton, exposed to the south of the CACB, comprises the Archean Zimbabwe and Kaapvaal cratons  
207 and grew by prolonged crustal accretion in the Palaeoproterozoic-Mesoproterozoic, amalgamating terranes such as  
208 the Choma-Kalomo Block, the Chewore Terrane and the Kaourera Terrane (Goscombe et al., 2020). The overlying  
209 Sijarira Group molasse contains  $570$  Ma to  $\sim 515$  Ma detrital zircons, and can be correlated with the Kundelungu Group  
210 on the northern foreland (Foster and Goscombe, 2013).

## 211 4 Tectonic Synthesis

### 212 4.1 Similarities to other orogens

213 The CACB exhibits many characteristics common to well-documented collisional orogens, in particular the spatial-  
214 temporal succession of lithologic assemblages and superimposed tectonothermal events (Figure 3). South of the  
215 Congo Craton and the undeformed foreland sedimentary rocks of the Katangan Basin, the External Fold-Thrust Belt  
216 of the Lufilian Orogen is characterized by low-grade metamorphism and pervasive thrust deformation. This resem-  
217 bles foreland systems such as the deformational front of the Appalachian-Caledonide system (negligible to low-grade  
218 metamorphism) and the Lesser Himalaya (typically greenschist facies) (Searle, 2022). However, the concentration  
219 of strain above salt-rich detachments is more akin to that in the Southern Pyrenees (e.g., Cámar and Flinch, 2017)  
220 and the Salt Range of Pakistan (e.g., Ghazi et al., 2015).

221 Progressing structurally upward and into the hinterland, the Domes Region records a markedly higher metamor-  
222 phic grade, with both right-way-up and inverted metamorphic sequences progressing from biotite- to kyanite-grade  
223 conditions (Ridgway and Ramsay, 1986) and locally attaining partial melting—a typical Barrovian-type sequence.  
224 This architecture mirrors that of the Greater Himalayan Sequence and the Moine metamorphic rocks of the Scottish  
225 Caledonides (Searle, 2022). The pressure–temperature (P–T) conditions recorded in the Domes Region range from  
226  $550$ – $800$  °C and  $6$ – $13$  kbar, closely matching those observed in the Greater Himalayan Sequence of the Himalayan oro-  
227 gen (Waters, 2019) (Figure 2). These pressures correspond to burial depths of approximately  $45$  km—far beyond what  
228 can be achieved through sedimentary loading—and instead require substantial crustal shortening and thickening

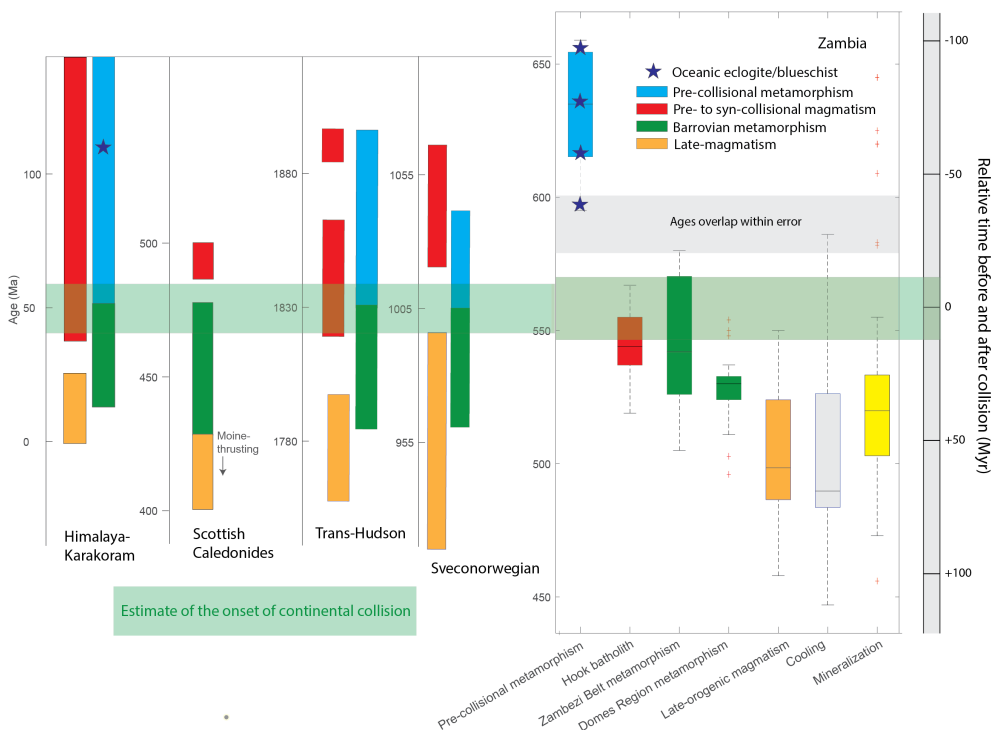


**Figure 3** Geochronological comparison between the CACB and other Himalayan-scale orogens. The evolution of the Trans-Hudson and Sveconorwegian orogens are taken from [Weller et al. \(2021\)](#), the evolution of the Himalaya-Karakoram from [St-Onge et al. \(2006\)](#), and the evolution of Scottish Caledonides from [Searle \(2022\)](#).

229 associated with the collision between the Congo and Kalahari continental plates. Peak metamorphism occurred at  
 230 ~530 Ma, coinciding with peak metamorphism in other regions involved in the assembly of Gondwana ([Cawood and](#)  
 231 [Buchan, 2007](#)).

232 The Lufilian Suture Zone closely resembles the Tethyan Sequence and Indus-Tsangpo Suture Zone of the Hi-  
 233 malaya: both exhibit epizonal- to amphibolite-grade metamorphism ([Dunkl et al., 2011](#)), contain dismembered ophi-  
 234 olitic fragments and subduction-related blueschist- to eclogite-facies rocks ([John et al., 2003; O'Brien, 2019](#)), and  
 235 record foreland-directed thrusting that steepens and then overturns toward the hinterland ([Corfield and Searle,](#)  
 236 [2000](#)). Similar features are also seen in the suture zone of the Scottish Caledonides ([Searle, 2022](#)). The 650–595 Ma  
 237 eclogites of the Zambezi Belt record metamorphic conditions equivalent to burial depths of up to 80 km and are fully  
 238 consistent with those of oceanic eclogites worldwide (Figure 2), necessitating a phase of oceanic subduction prior to  
 239 continent-continent collision ([John et al., 2003](#)). This is akin to the 100 Ma blueschists of Ladakh in the Himalayan  
 240 orogen ([O'Brien, 2019](#)).

241 The Zambezi Belt preserves evidence of medium-temperature–medium-pressure metamorphism coeval with this  
 242 period of oceanic subduction. Regional metamorphism prior to continent-continent collision is well documented in  
 243 orogenic systems. For example, the Karakoram experienced amphibolite-grade metamorphism during the Creta-  
 244 ceous ([Fraser et al., 2001](#)). In the North American Cordillera, significant crustal thickening and high-grade metamor-  
 245 phism during the Laramide Orogeny were driven by flat-slab subduction in the Late Cretaceous to Paleocene, result-  
 246 ing from increased traction along the plate interface and enhanced end-loading at the trench ([Yonkee and Weil, 2015](#)).  
 247 This mechanism has also been suggested for the Scottish Caledonides ([Lamont et al., 2025](#)). The Lufilian Suture Zone  
 248 then experienced substantial crustal thickening up to 12 kbar during the subsequent continent-continent collision.

249 This began at 570 Ma and progressed through to 530 Ma, coinciding with peak metamorphism of comparable grade  
250 in the Domes Region.

251 The Hook Batholith is the only pre- to syn-collisional magmatism recorded in the CACB. The lack of pre-collisional  
252 calc-alkaline magmatic arc preserved in Zambia has caused confusion. It should be noted that well-known collisional  
253 zones which previously experienced oceanic subduction, such as the Alps, do not contain such an arc (McCarthy et al.,  
254 2018), and it is almost certain that any subduction-related magmatic arc would now underlay the Lufilian Suture  
255 Zone. The CACB also exhibits late-stage magmatism and thrusting, which overlap with and postdate peak crustal  
256 thickening. For example, syenites are observed cropping out in the Domes Region (Cosi et al., 1992) and granitic  
257 pegmatites are found in the External Fold-Thrust Belt (Seifert et al., 2004). These intrusions, aged between  $\sim$  534–  
258 465 Ma, are contemporaneous with high-temperature metamorphism and granite magmatism documented in other  
259 parts of the Gondwana assembly (Cawood and Buchan, 2007). The intrusion of late-stage granites is analogous to the  
260 “Newer Granites” of the Scottish Caledonides (Pankhurst and Sutherland, 1982), as well as the 960–935 Ma granitic  
261 pegmatites in the Sveconorwegian orogen (Möller et al., 2007). Finally, to the north and south of the Lufilian Orogen  
262 lie the Plateau Group and Sijairi molasses, respectively. These are akin to the Siwalik molasse basin which formed  
263 along the southern margin of the Himalaya during the uplift of the mountain chain (St-Onge et al., 2006).

## 264 4.2 A new model for the CACB

265 The tectonic evolution of the CACB can be divided into several phases indicative of a typical Wilson Cycle. Figure 4  
266 provides a schematic illustration of this evolution, beginning with the onset of subduction. The numbered stages in  
267 Figure 4 are referenced throughout the text as F4.1, ..., F4.N.

268 **Continental extension (880–765 Ma)** Extension between the Congo and Kalahari cratons began at a maximum of  
269 880 Ma, as constrained by the age of the Nchanga granite which unconformably underlies the CACB (Armstrong  
270 et al., 2005). This extension provided accommodation space for the deposition of the Lower and Upper Roan Group  
271 sedimentary rocks in the CACB and the lowermost units of the Zambezi Supercrustal Group (F4.2) (Purkiss, 2025;  
272 Johnson et al., 2007; Daly et al., 2025). Minor igneous units were intruded during this time, including the Ngoma  
273 Gneiss and the Munali ultramafic body (Holwell et al., 2017).

274 **Ocean basin formation (765–650 Ma)** A second phase of rifting is preserved in the Mwashia Group of the CACB,  
275 during which there was extensive mafic magmatism (Purkiss, 2025). This period is interpreted to record the final  
276 stages of continental breakup and the formation of oceanic crust. The increase in mafic magmatism prior to final  
277 rifting is commonly observed in rift settings (e.g., Sun et al., 2019). The size of the resulting ocean basin is largely  
278 unconstrained (F4.1) but must have been relatively sizeable as the Congo and Kalahari craton margins become distinct  
279 entities with contrasting palaeomagnetic and detrital zircon records (Foster and Goscombe, 2013; Goscombe et al.,  
280 2020).

281 **Oceanic subduction and pre-collisional metamorphism (650 Ma onwards)** Oceanic subduction began sometime  
282 during the Cryogenian, evidenced by the  $\sim$  650 Ma eclogites preserved in the Zambezi Belt of the Lufilian Suture  
283 Zone (F4.3) (John et al., 2004). Today, the eclogites are found in close relationship with oceanic metasedimentary

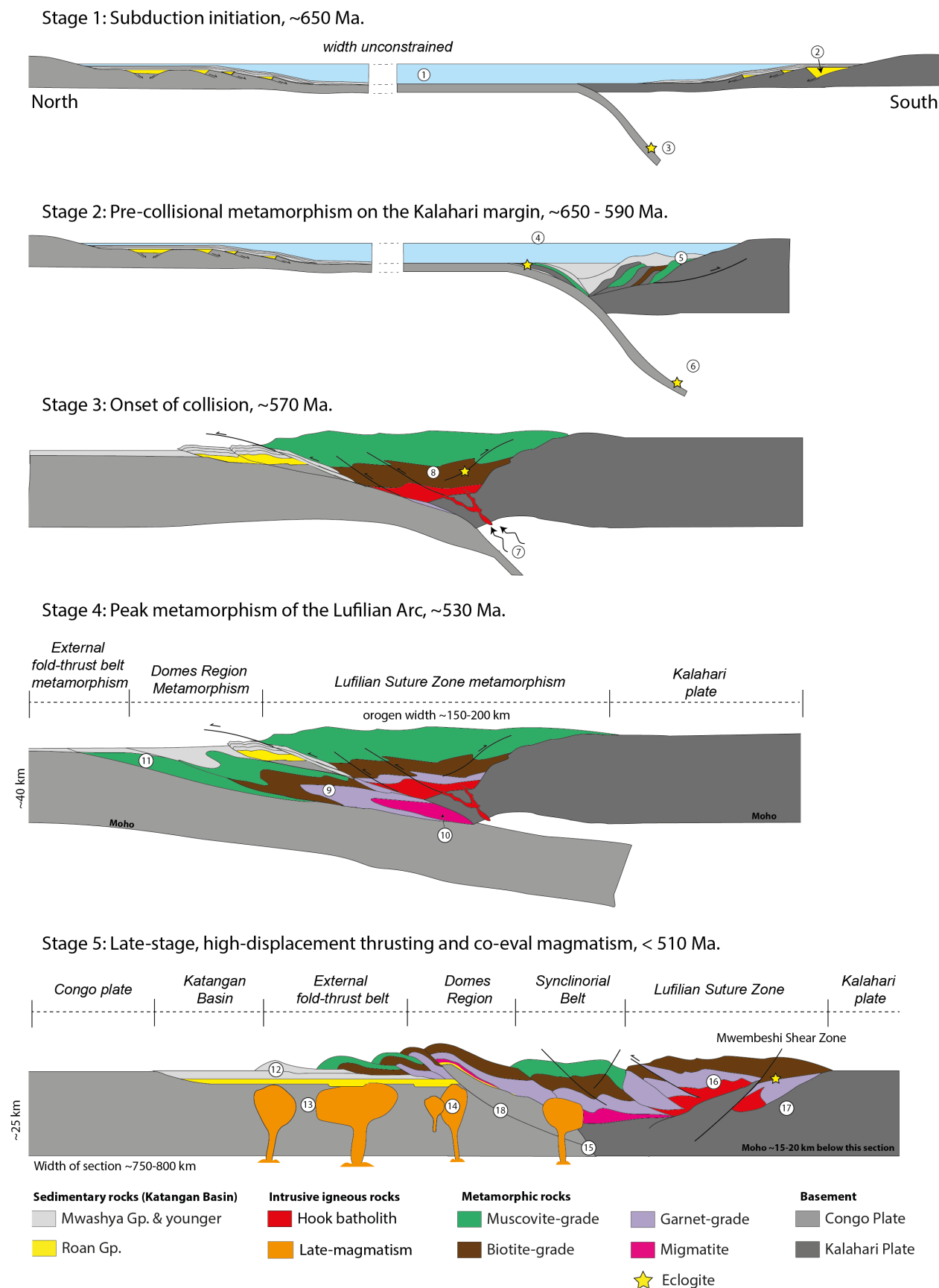


**Figure 4** Tectonic model of the CACB.

284 rocks and ophiolitic fragments (F4.4). With metamorphic conditions of  $\sim 540$ – $550$  °C and  $\sim 21$ – $23$  kbar, these eclogites clearly preserve a subduction geotherm (John et al., 2003; Goscombe et al., 2020). Eclogite-facies metamorphism continued until  $595 \pm 10$  Ma (John et al., 2003) (F4.6). Concurrent with oceanic subduction, the Kalahari Plate underwent medium-temperature/medium-pressure metamorphism at  $570$ – $665$  °C and  $6.5$ – $9$  kbar from  $656 \pm 16$  Ma– $635 \pm 2$  Ma (Fig. 4.5; Sakuwaha et al., 2022).

289 **Onset of collision (~570 Ma)** The exact timing of collision is still a point of significant debate in well-preserved, 290 modern orogens such as the Himalaya (Hu et al., 2016). Consequently, it is unlikely we will be able to resolve the 291 exact timing of collision in the CACB. However, a new period of garnet-grade conditions and metamorphic monazite 292 growth are recorded in the Zambezi Belt at  $\sim 570$  Ma (F4.8) (Johnson et al., 2007; Sakuwaha et al., 2022). The Hook 293 Batholith magmatism also began at this time as a result of crustal and mantle fluid-flux melting (Milani et al., 2015). 294 These melts would have intruded the overlying metasedimentary rocks of the Lufilian Suture Zone and the Kalahari 295 plate (F4.7).

296 **Peak metamorphism (~530 Ma)** Peak metamorphic conditions in both the Domes Region and the Lufilian Suture 297 Zone were attained at  $\sim 530$  Ma (e.g., John et al., 2004; Eglinger et al., 2016; Naydenov et al., 2016). The Domes Region 298 progressed into a significant orogenic wedge akin to the Greater Himalayan Sequence (F4.9). Metamorphic conditions 299 reached kyanite-grade, with preserved evidence of partial melting (F4.10) (Eglinger et al., 2016). The External 300 Fold-Thrust Belt experienced greenschist-facies metamorphism (F4.11) (Rainaud et al., 2005). The molasse of the 301 Kundelungu (north) and the Sijarira Group (south) formed as the result of erosion during exhumation of the inter- 302 vening orogenic core.

303 **Late-thrusting and magmatism (< 510 Ma)** Following peak metamorphism, the orogenic belt experienced significant 304 lateral transport towards both the south and north. This is evidenced by the preservation of kyanite-grade 305 metasedimentary rocks directly atop autochthonous undeformed sedimentary rocks in the Domes Region (Daly et al., 306 2025). The timing of this event is not well constrained but likely occurred at  $\sim 510$  Ma as evidenced by zircon over- 307 growths in the autochthonous lithologies (Barron, 2003). The most significant transport occurred in the External 308 Fold-Thrust Belt, characterized by northward thin-skinned thrusting and imbrication of the Katangan Supergroup 309 stratigraphy above evaporite-rich detachments (Coward and Daly, 1984). These lubricated detachments accommodated 310 lateral transport of up to  $65$ – $150$  km northwards (F4.12) (Porada and Berhorst, 2000; Jackson et al., 2003). These 311 significant displacements and the curvilinear thrusting related to the syntaxis geometry of the orogen explain the 312 significant across-strike width of the CACB, comparable to that observed in the western syntaxis of the Himalaya in 313 Pakistan (e.g., Ghazi et al., 2015). The late-stage thrusting also involved thick-skinned, out-of-sequence exhumation 314 of basement rocks in the Domes Region and the Zambezi Belt (Fig. 4.12). This is observed in the Moine Thrust Zone 315 of the Scottish Caledonides, with out-of-sequence thrusting of basement Lewisian Gneiss over Cambro-Ordovician 316 sedimentary rocks (e.g., Searle et al., 2019). Similar observations can be made in the fold-and-thrust belts of the 317 Appalachian and Grenvillian orogenic fronts (van Gool et al., 2008).

318 Late-thrusting was coeval with the intrusion of granites and syenites (F4.13). Syenites are observed cropping out

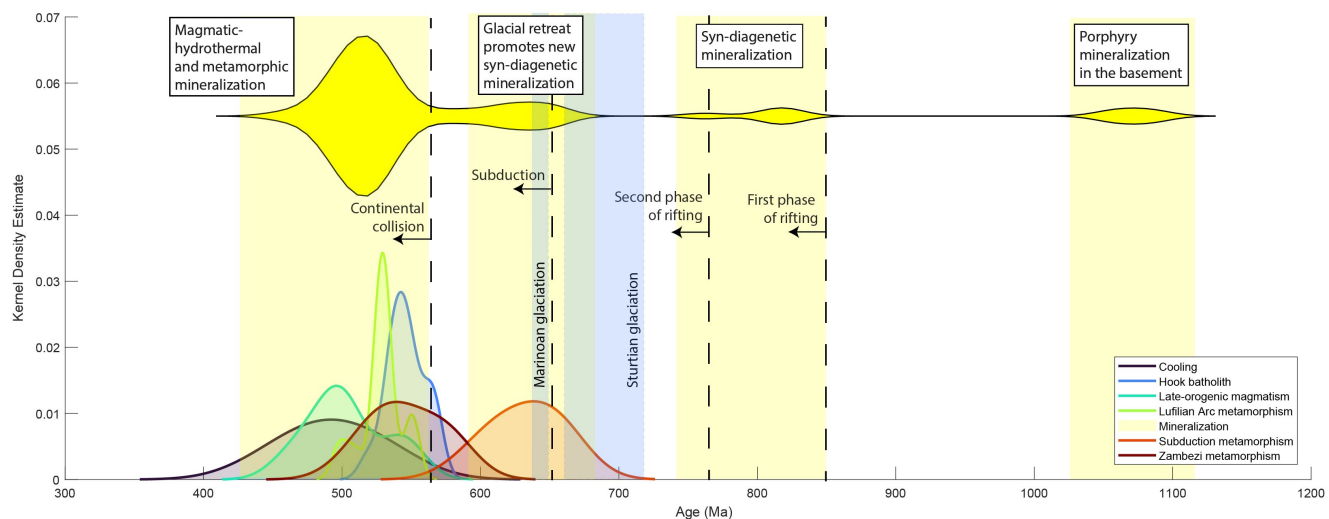


**Figure 5** Mineralization and tectonothermal events in the CACB. The timing of the Snowball Earth glaciations were taken from Hoffman et al. (2017), the timing of the two rifting events was taken from Purkiss (2025).

319 in the Domes Region (Cosi et al., 1992) and into the Southern Irumide Belt (footwall of the CACB) between 534–465 Ma  
 320 (Johnson et al., 2006). Lufilian-age granitic pegmatites are also found in the Domes Region (F4.14) (Selley et al., 2018)  
 321 and the External Fold-Thrust Belt (Seifert et al., 2004). The observed change in the direction and magnitude of mantle  
 322 anisotropy indicates that the Congo–Kalahari craton boundary now lies beneath the Synclinorial Belt (Kounoudis  
 323 et al., 2024) (F4.15). The Mwombeshi Shear Zone is interpreted as a late, right-lateral, oblique-slip fault with a reverse  
 324 component (F4.17), which has likely helped to exhume the Hook batholith. Late Lufilian-age IOCG, lode-gold and  
 325 hydrothermal metal deposits are found neighbouring the Hook (F4.15) (Milani et al., 2015).

326 **Post-orogenic uplift and cooling (< 500 Ma)** The abundance of mica cooling ages indicates post-orogenic uplift  
 327 began at ~500 Ma. This is supported by zircon fission-track thermochronometry from sandstones in Solwezi (NW  
 328 Zambia) which shows that uplift took place from 500–400 Ma (Daly et al., 2025). Granitoids continued to be intruded  
 329 during this period (Johnson et al., 2006).

## 330 5 The mineral system of the CACB

331 A Kernel Density Estimation of geochronological ages from mineralized and coeval phases in deposits around the  
 332 CACB was used to characterize the temporal distribution of mineralization and its relationship to tectonic events  
 333 (Figure 5). This analysis demonstrates that there are four key periods of mineralization. Firstly, there is evidence of  
 334 appreciable Mesoproterozoic mineralization in the basement of the CACB at  $1084\text{--}1059 \pm 5$  Ma (Sillitoe et al., 2015;  
 335 Master and Ndhlovu, 2019). This is thought to be the result of porphyry-systems active during the Irumide Orogeny  
 336 (Rainaud et al., 2005), and is a key source of metals for the overlying Katangan Basin (Cailteux et al., 2005).

337 Secondly, there is evidence of syn-diagenetic mineralization of Katangan Supergroup sedimentary rocks within  
 338 the External Fold-Thrust Belt. For example, the Kamoto deposit of the DRC contains mineralization dated at  $821 \pm$   
 339 51 and  $762 \pm 33$  Ma (Muchez et al., 2015). The “red-bed” model is currently the prevailing genetic framework for syn-  
 340 diagenetic mineralization in the CACB (Hitzman et al., 2005). This model posits that metal deposits formed through  
 341 the migration of oxidized, metal-rich basinal fluids into reduced lithologies—typically carbonaceous shales—during

342 sediment deposition and diagenesis. These metals are thought to originate from the chemical leaching of red-bed  
343 sedimentary sequences within the Katangan Basin. The KDE analysis indicates that syn-diagenetic deposits con-  
344 tribute only marginally to the CACB's metal budget by deposit count, challenging traditional interpretations.

345 Thirdly, there is evidence of a pulse of mineralization from  $\sim$  652–609 Ma (Saintilan et al., 2018; Cahen, 1961; De-  
346 crée et al., 2011). Mineralization of this age is preserved across the Domes Region and External Fold-Thrust Belt,  
347 including Ndola (Cahen, 1961), Musoshi (Richards et al., 1988), and Kamoto (Saintilan et al., 2018). This overlaps  
348 with the age of the earliest eclogite-facies metamorphism in the CACB (John et al., 2003), suggesting that this min-  
349 eralization could be the result of crustal re-arrangement during oceanic subduction. However, the mineralization  
350 is not preserved within the Lufilian Suture Zone. Instead, this mineralization is perhaps the impact of deglaciation  
351 following the Marinoan Snowball Earth event (Saintilan et al., 2018) (Figure 5). Glacial retreat would have resulted  
352 in increased erosion of the continent and a resultant renewed influx of metals into the Katangan Basin (Parnell and  
353 Boyce, 2019). These metals would have been deposited in a hypersaline, euxinic ocean (Scheller et al., 2018), a set-  
354 ting known to have promoted substantial pyrite deposition (Sansjofre et al., 2016)—ideal conditions for generating  
355 metal-rich basinal brines and the deposition of syn-diagenetic copper-sulfide deposits at redox boundaries within  
356 the basin.

357 Finally, the most significant mineralization event in the basin occurred between  $\sim$  560–470 Ma (Sillitoe et al., 2017).  
358 Some studies have argued that this mineralization reflects a metamorphic recrystallisation of syn-diagenetic min-  
359 eralization during the Lufilian orogeny (e.g., Turlin et al., 2016). However, Sillitoe et al. (2017) argue that the ages  
360 reflect a new mineralization event during the Lufilian Orogeny, as molybdenite and copper minerals can withstand  
361 amphibolite-grade metamorphism without re-mobilization or isotopic resetting (Sillitoe et al., 2015). Similarly, Tor-  
362 realday (2000) propose that the mineralized veins in the Kansanshi Cu-Au mine, NW Zambia, are metamorphic in  
363 origin. Within the context of the new tectonic framework, these observations point to shortening and crustal thick-  
364 ening during orogenesis as key drivers in the formation of metal deposits, through the development of a thermal  
365 and stress regime that enables widespread fluid mobilization. These oxidized metamorphic fluids would have scav-  
366 enged metals from the orogenic wedge and surrounding sedimentary and basement rocks, precipitating them at  
367 redox boundaries. This accounts for the cluster of mineralization events around the time of peak metamorphism at  
368  $\sim$  530 Ma and potentially throughout the ensuing 10s Myrs during exhumation and cooling. However, it seems clear  
369 that syn- to late-orogenic magmatism played a significant role in the formation of metal deposits in the CACB, and  
370 provides a more compelling explanation for the concentration of mineralization dated at  $\leq$  510 Myr in particular.

### 371 5.1 Evidence for the magmatic origins of CACB mineralization

372 There are three primary lines of evidence, outlined below, which indicate that magmatism contributed new fluids,  
373 metals, and thermal energy to the mineral system of the CACB syn- to post-Lufilian orogeny. It should be noted that  
374 this is not without precedent: magmatic-hydrothermal systems overlying granite plutons have been identified as the  
375 root of multi-stage REE-Y-Co-Cu-Au sediment-hosted mineralization in the Idaho Cobalt Belt of the Belt-Purcell Basin,  
376 USA (Saintilan et al., 2018).

**377 The characteristics of existing deposits** Late-stage mineralization, occurring after peak metamorphism, has been  
378 associated with high-temperature ( $\leq 400$  °C), high-salinity fluids, variably attributed to magmatic sources (El Desouky  
379 et al., 2009; Greyling, 2009; Annels, 1989). This interpretation is supported by juvenile osmium isotope signatures  
380 in the Kamoto deposit and sulfur isotope data from the Samba deposit, both of which require a magmatic origin  
381 (Saintilan et al., 2018; Zhang et al., 2023). Indeed, the brines in the CACB display Cu concentrations overlapping  
382 those of magmatic-hydrothermal systems (Davey et al., 2020).

**383** These geochemical signatures align with the known characteristics of several magmatic-related deposits in the  
384 region. The Hook Batholith, for instance, hosts iron-oxide-copper-gold (IOCG) deposits (Milani et al., 2019), and the  
385 External Fold-Thrust Belt hosts Lufilian-age pegmatites linked to emerald mineralization (Seifert et al., 2004). This  
386 belt also contains magmatic-hydrothermal Cu-Au mineralization dated to 530–517 Ma (Perelló et al., 2022), and the  
387 Kipushi Mine (Zn-Pb-Cu) in the DRC has been similarly attributed to underlying magmatic activity (Walraven and  
388 Chabu, 1994; Heijlen et al., 2008). A magmatic source has also been proposed for cobalt mineralization in the CACB  
389 (Annels et al., 1983). Moreover, many CACB deposits exhibit structural and mineralogical features inconsistent with  
390 syn-diagenetic or metamorphic models. Instead of standard disseminated textures or small veinlets, deposits such  
391 as Kansanshi, Kalengwa, and Safari contain large, cross-cutting, metal-rich veins (Taylor et al., 2013)—often over a  
392 metre wide—indicative of a late-stage, high-intensity hydrothermal system.

**393 Temporal correlation between granitic intrusions and mineral deposits** Mineralization in the CACB predomi-  
394 nantly occurred from  $\sim$ 530–490 Ma, with some deposits as late as 465 Ma (Sillitoe et al., 2017). This time frame over-  
395 laps entirely with the intrusion of granites and syenites into the Irumide Belt (534–465 Ma; Johnson et al., 2006),  
396 which appears along strike and forms the footwall to the CACB (Figure 1). It also correlates with Lufilian-age alkali-  
397 granites/syenites in the Domes Region (Cosi et al., 1992) and granitic pegmatites in the External Fold-Thrust Belt  
398 (Seifert et al., 2004). Indeed, the ages of mineralization during the Lufilian appear to show the strongest correlation  
399 with magmatism rather than metamorphism or cooling (Figure 3). Based on this timing and structural correlation,  
400 it should be expected that late-magmatism would provide a significant control on the mineral system of the CACB.

**401 Localization of distinct metal suites** Another striking feature of the CACB is the highly localized distribution of  
402 metal suites along strike, and indeed the large variety in metal contents (Cu, Au, Ag, Pb, Ni, Co, etc.) and mineral-  
403 ization styles. For example, the Kansanshi deposit in the Domes Region hosts both copper and gold in a vein-style  
404 system, yet gold is entirely absent at the supergiant Cu-only Sentinel mine, located  $\sim$ 100 km along strike. Gold then  
405 reappears at the Kasenseli Gold Mine near Mwinilunga, a further  $\sim$ 100 km along strike (data sourced from publicly  
406 available mining reports). Even more starkly, the Cu-dominant, Ni-absent Sentinel deposit lies just  $\sim$ 10 km along  
407 strike from the Enterprise mine, which hosts abundant hydrothermal nickel but only minor copper mineralization  
408 (Capistrant et al., 2015). If such abrupt changes in metal assemblages and mineralization styles were purely sedi-  
409 mentary in origin, it would necessitate a highly segmented basin, with discrete sub-basins on the scale of tens of  
410 kilometres, each with a unique metal source. This is an unlikely scenario, particularly given the requirement for  
411 high-tonnage, distinct metal sources. An alternative explanation proposed here is that the metals originated from  
412 underlying metal-bearing intrusions, with variability in metal assemblages reflecting the spatial distribution and

413 metal content of these bodies (Darnley, 1960; Gray, 1929). For example, the Zn-Pb-Cu deposit at Kipushi has been  
414 attributed to magmatism (see above). Likewise, perhaps the Ni enrichment at the Enterprise deposit reflects input  
415 from an underlying syenite and mafic/ultramafic intrusion—potentially a satellite body related to the larger granitoid  
416 system responsible for Cu mineralization at Sentinel. Syenites are recognized sources of Ni, as demonstrated in the  
417 Scottish Caledonides (Graham et al., 2017), and are commonly spatially associated with ultramafic intrusions, as in  
418 Myanmar (Searle et al., 2020).

## 419 5.2 Anomalous nature of the CACB mineral system

420 Ultimately, the anomalous metal endowment of the CACB reflects a combination of factors. First, erosion of a pre-  
421 enriched basement would have contributed substantial metal content to the rift-related sedimentary rocks of the  
422 Katangan Basin. Second, the prolonged geological evolution of the CACB—from ~880 Ma to < 500 Ma—allowed ample  
423 time for large-scale hydrothermal circulation, metal transport and deposition. Thirdly, the evaporite-rich sedimentary  
424 rocks of the Katangan Basin served as a substantial source of sulfur essential for the development of metalliferous  
425 basinal brines. Finally, magmatism during and after continent-continent collision introduced a new pulse of heat,  
426 metals, and fluids into an already enriched system. As such, the CACB possesses two distinct metal sources: metals  
427 derived from the erosion of the basement and those introduced by magmatism during and after continent-continent  
428 collision. The metal-rich character of this magmatism is unsurprising, given that the CACB basement previously  
429 generated metal-bearing granites during the Mesoproterozoic (Sillitoe et al., 2015).

## 430 6 Conclusions

431 This study reinterprets the Central African Copperbelt (CACB) as a Himalayan-scale, continental-collision orogenic  
432 system, characterized by a full Wilson Cycle spanning over 400 million years. The region evolved from continental  
433 rifting (~880 Ma), through ocean basin formation (765–650 Ma), subduction and eclogite-facies metamorphism  
434 (650–595 Ma), to continental collision (~570 Ma), with peak crustal thickening and metamorphism at ~530 Ma (up  
435 to 13 kbar or ~45 km burial). The new geodynamic model is consistent with structural, petrological, geochronological,  
436 and geophysical data, and provides a coherent explanation for the observed regional metamorphism and  
437 magmatism—features that are not easily reconciled within the traditional sedimentary-basin framework.

438 The dominant mineralization event occurred between ~560–470 Ma, overlapping with peak metamorphism and  
439 late-stage thrusting, and temporally coinciding with widespread intrusion of granites and syenites (534–465 Ma).  
440 Three lines of evidence support the critical role of magmatism during and after continent-continent collision in  
441 metal sourcing, transport and deposition: (1) geochemical and isotopic signatures indicate the presence of hot, high-  
442 salinity mineralizing fluids derived from magmatic intrusions; (2) the timing and structural position of mineral-  
443 ization strongly correlates with granite and syenite intrusions across the Domes Region, External Fold-Thrust Belt,  
444 and the Irumide Belt; and (3) localized variations in metal assemblages—for example, the Cu-dominant, Ni-absent  
445 Sentinel deposit and the nearby Ni-dominant, Cu-poor Enterprise deposit just 10 km apart—strongly suggest that  
446 mineralization was controlled by spatially heterogeneous, metal-bearing magmatic intrusions rather than uniform  
447 sedimentary processes.

448 The CACB today hosts some of the world's most significant sediment-hosted deposits—including Kansanshi (1,125.4 Mt

449 Cu), Sentinel (648.7 Mt Cu), and Konkola ( $\geq$ 140.3 Mt Cu)—and supplies  $\sim$ 14 % of global copper and  $\sim$ 60 % of cobalt.  
450 The combination of a pre-enriched basement, evaporite-rich sedimentary sequences, prolonged tectonothermal evo-  
451 lution, and late-stage magmatism accounts for this exceptional endowment. The new geodynamic model establishes  
452 a framework for mineral exploration in the CACB and analogous collisional belts worldwide, and indicates that the  
453 CACB benefitted from two principal metal sources: metals derived from basement erosion and those introduced by  
454 magmatism during and after continent–continent collision. The model predicts that the next generation of metal  
455 deposits in the CACB will be found by locating outcropping or shallow subsurface magmatic intrusions.

456 **Acknowledgements**

457 I gratefully acknowledge John-Michael Kendall for funding my post-doctoral research at the University of Oxford. I  
458 am indebted to Chris Hawkesworth, Ian Cawood, Peter Cawood, Martin Purkiss, Mike Searle, and Rita Kounoudis for  
459 their invaluable comments on earlier drafts of this manuscript. Thanks also to Michael Daly, Laurence Robb, and  
460 Tony Watts for engaging discussions on the tectonics of Zambia over the years. I declare no competing interests. All  
461 data are available in the manuscript or the supplementary materials.

462 **References (= 100 total)**

463 Annels, A. Ore genesis in the Zambian copperbelt, with particular reference to the northern sector of the Chambishi Basin. *Geological*  
464 *Association of Canada Special Paper*, 36:427 – 452, 1989.

465 Annels, A., Vaughan, D., and Craig, J. Conditions of ore mineral formation in certain Zambian Copperbelt deposits with special reference  
466 to the role of cobalt. *Mineralium Deposita*, 18(1), apr 1983. doi: 10.1007/BF00206696.

467 Armstrong, R., Master, S., and Robb, L. Geochronology of the Nchanga Granite, and constraints on the maximum age of the Katanga Super-  
468 group, Zambian Copperbelt. *Journal of African Earth Sciences*, 42(1-5):32–40, jul 2005. doi: 10.1016/j.jafrearsci.2005.08.012.

469 Barron, J. W. *The Stratigraphy, Metamorphism, and Tectonic History of the Solwezi Area, Northwest Province, Zambia: Integrating Geological*  
470 *Field Observations and Airborne Geophysics in the Interpretation of Regional Geology*. PhD thesis, Colorado School of Mines, 2003.

471 Cahen, L. Review of Geochronological Knowledge in Middle and Northern Africa. *Annals of the New York Academy of Sciences*, 91(2):535–566,  
472 1961. doi: <https://doi.org/10.1111/j.1749-6632.1961.tb35519.x>.

473 Cailteux, J., Kampunzu, A., Lerouge, C., Kaputo, A., and Milesi, J. Genesis of sediment-hosted stratiform copper–cobalt deposits, central  
474 African Copperbelt. *Journal of African Earth Sciences*, 42(1-5):134–158, July 2005. doi: 10.1016/j.jafrearsci.2005.08.001.

475 Capistrant, P. L., Hitzman, M. W., Wood, D., Kelly, N. M., Williams, G., Zimba, M., Kuiper, Y., Jack, D., and Stein, H. Geology of the Enterprise  
476 Hydrothermal Nickel Deposit, North-Western Province, Zambia. *Economic Geology*, 110(1):9–38, 01 2015. doi: 10.2113/econgeo.110.1.9.

477 Cawood, P. A. and Buchan, C. Linking accretionary orogenesis with supercontinent assembly. *Earth-Science Reviews*, 82(3):217–256, 2007.  
478 doi: <https://doi.org/10.1016/j.earscirev.2007.03.003>.

479 Chen, Y., Ye, K., Wu, T. F., and Guo, S. Exhumation of oceanic eclogites: thermodynamic constraints on pressure, temperature, bulk compo-  
480 sition and density. *Journal of Metamorphic Geology*, 31(5):549–570, 2013. doi: <https://doi.org/10.1111/jmg.12033>.

481 Corfield, R. I. and Searle, M. P. Crustal shortening estimates across the north Indian continental margin, Ladakh, NW India. *Geological*  
482 *Society, London, Special Publications*, 170(1):395–410, 2000. doi: 10.1144/GSL.SP.2000.170.01.21.

483 Cosi, M., De Bonis, A., Gosso, G., Hunziker, J., Martinotti, G., Moratto, S., Robert, J., and Ruhlman, F. Late proterozoic thrust tectonics, high-  
484 pressure metamorphism and uranium mineralization in the Domes Area, Lufilian Arc, Northwestern Zambia. *Precambrian Research*, 58  
485 (1-4):215–240, oct 1992. doi: 10.1016/0301-9268(92)90120-D.

486 Coward, M. P. and Daly, M. C. Crustal lineaments and shear zones in Africa: Their relationship to plate movements. *Precambrian Research*,  
487 24(1):27–45, feb 1984. doi: 10.1016/0301-9268(84)90068-8.

488 Cámar, P. and Flinch, J. Chapter 18 - The Southern Pyrenees: A Salt-Based Fold-and-Thrust Belt. In Soto, J. I., Flinch, J. F.,  
489 and Tari, G., editors, *Permo-Triassic Salt Provinces of Europe, North Africa and the Atlantic Margins*, pages 395–415. Elsevier, 2017.  
490 doi: <https://doi.org/10.1016/B978-0-12-809417-4.00019-7>.

491 Daly, M. C., Zimba, M., Purkiss, M., and Chibesakunda, F. The Inter-Cratonic Neoproterozoic Katangan Basin of Central  
492 Africa: Rift Basin Formation, Orogenic Inversion and Potential Fluid Pathways. *Tectonics*, 44(7):e2025TC008955, 2025.  
493 doi: <https://doi.org/10.1029/2025TC008955>.

494 Darnley, A. Petrology of some Rhodesian Copperbelt orebodies and associated rocks. *Institute of Mining and Metallurgy Transactions*, 69:  
495 137–173, 1960.

496 Davey, J., Roberts, S., and Wilkinson, J. J. Copper- and cobalt-rich, ultrapotassic bittern brines responsible for the formation of the Nkana-  
497 Mindola deposits, Zambian Copperbelt. *Geology*, 49(3):341–345, 11 2020. doi: 10.1130/G48176.1.

498 De Swardt, A. M. J., Drysdall, A. R., and Garrard, P. Precambrian geology and structure in central Northern Rhodesia. *Northern Rhodesia*,

499 geological Survey, *Memoir*, (2), 1964.

500 Decrée, S., Étienne Deloule, De Putter, T., Dewaele, S., Mees, F., Yans, J., and Marignac, C. SIMS U-Pb dating of uranium  
501 mineralization in the Katanga Copperbelt: Constraints for the geodynamic context. *Ore Geology Reviews*, 40(1):81–89, 2011.  
502 doi: <https://doi.org/10.1016/j.oregeorev.2011.05.003>.

503 Dirks, P., Kröner, A., Jelsma, H., Sithole, T., and Vinyu, M. Structural relations and Pb-Pb zircon ages for the Makuti gneisses: evidence for a  
504 crustal-scale Pan-African shear zone in the Zambezi Belt, northwest Zimbabwe. *Journal of African Earth Sciences*, 28(2):427–442, 1999.  
505 doi: [https://doi.org/10.1016/S0899-5362\(99\)00013-5](https://doi.org/10.1016/S0899-5362(99)00013-5).

506 Dominish, E., Florin, N., and Teske, S. Responsible Minerals Sourcing for Renewable Energy. Technical report, Institute for Sustainable  
507 Futures, University of Technology Sydney., 2019.

508 Dunkl, I., Antolín, B., Wemmer, K., Rantitsch, G., Kienast, M., Montomoli, C., Ding, L., Carosi, R., Appel, E., El Bay, R., Xu, Q., and Von Eynatten,  
509 H. Metamorphic evolution of the Tethyan Himalayan flysch in SE Tibet. *Geological Society, London, Special Publications*, 353(1):45–69,  
510 jan 2011. doi: 10.1144/SP353.4.

511 Eglinger, A., André-Mayer, A.-S., Vanderhaeghe, O., Mercadier, J., Cuney, M., Decrée, S., Feybesse, J.-L., and Milesi, J.-P. Geochemical sig-  
512 natures of uranium oxides in the Lufilian belt: From unconformity-related to syn-metamorphic uranium deposits during the Pan-African  
513 orogenic cycle. *Ore Geology Reviews*, 54:197–213, 2013. doi: <https://doi.org/10.1016/j.oregeorev.2013.04.003>.

514 Eglinger, A., Vanderhaeghe, O., André-Mayer, A. S., Goncalves, P., Zeh, A., Durand, C., and Deloule, E. Tectono-metamorphic evolution  
515 of the internal zone of the Pan-African Lufilian orogenic belt (Zambia): Implications for crustal reworking and syn-orogenic uranium  
516 mineralizations. *Lithos*, 240–243:167–188, 2016. doi: 10.1016/j.lithos.2015.10.021.

517 El Desouky, H. A., Muchez, P., and Cailteux, J. Two Cu–Co sulfide phases and contrasting fluid systems in the Katanga Copperbelt, Demo-  
518 cratic Republic of Congo. *Ore Geology Reviews*, 36(4):315–332, 2009. doi: <https://doi.org/10.1016/j.oregeorev.2009.07.003>.

519 Foster, D. and Goscombe, B. Continental Growth and Recycling in Convergent Orogens with Large Turbidite Fans on Oceanic Crust. *Geo-  
520 sciences*, 3:354–388, 7 2013. doi: 10.3390/geosciences3030354.

521 Fraser, J. E., Searle, M. P., Parrish, R. R., and Noble, S. R. Chronology of deformation, metamorphism, and magmatism in the southern  
522 Karakoram Mountains. *GSA Bulletin*, 113(11):1443–1455, 11 2001. doi: 10.1130/0016-7606(2001)113<1443:CODMAM>2.0.CO;2.

523 Ghazi, S., Ali, S. H., Sahraeyan, M., and Hanif, T. An overview of tectonosedimentary framework of the Salt Range, northwestern Himalayan  
524 fold and thrust belt, Pakistan. *Arabian Journal of Geosciences*, 8:1635–1651, 3 2015. doi: 10.1007/s12517-014-1284-3.

525 Goscombe, B., Foster, D. A., Gray, D., and Wade, B. Assembly of central Gondwana along the Zambezi Belt: Metamorphic response and  
526 basement reactivation during the Kuunga Orogeny. *Gondwana Research*, 80:410–465, 2020. doi: 10.1016/j.gr.2019.11.004.

527 Graham, S., Holwell, D., McDonald, I., Jenkin, G., Hill, N., Boyce, A., Smith, J., and Sangster, C. Magmatic Cu-Ni-PGE-Au sulfide mineralisation  
528 in alkaline igneous systems: An example from the Sron Garbh intrusion, Tyndrum, Scotland. *Ore Geology Reviews*, 80:961–984, 2017.  
529 doi: <https://doi.org/10.1016/j.oregeorev.2016.08.031>.

530 Gray, A. The outline of the geology and ore deposits of the Nkana concession. In *International Geological Congress*, 1929.

531 Greyling, L. *Fluid evolution and characterisation of mineralising solutions in the Central African Copperbelt*. PhD Thesis, University of Witwa-  
532 tersrand, Johannesburg, 2009.

533 Hammarstrom, J. M., Zientek, M. L., Parks, H. L., Dicken, C. L., and U.S. Geological Survey Global Copper Mineral Resource Assessment Team.  
534 Assessment of undiscovered copper resources of the world, 2015. Technical report, US Geological Survey, 2019. <https://pubs.usgs.gov/publication/sir20185160>. ISSN: 2328-0328.

535 Hanson, R. E., Wilson, T. J., and Wardlaw, M. S. Deformed batholiths in the Pan-African Zambezi belt, Zambia: Age and implications for

537 regional Proterozoic tectonics. *Geology*, 16(12):1134, 1988. doi: 10.1130/0091-7613(1988)016<1134:DBITPA>2.3.CO;2.

538 Hanson, R. E., Wardlaw, M. S., Wilson, T. J., and Mwale, G. U-Pb zircon ages from the Hook granite massif and Mwembeshi dislocation:  
539 constraints on Pan-African deformation, plutonism, and transcurrent shearing in Central Zambia. *Precambrian Research*, 63(3):189–209,  
540 1993. doi: [https://doi.org/10.1016/0301-9268\(93\)90033-X](https://doi.org/10.1016/0301-9268(93)90033-X).

541 Heijlen, W., Banks, D. A., Muchez, P., Stensgard, B. M., and Yardley, B. W. D. The Nature of Mineralizing Fluids of the Kipushi Zn-Cu De-  
542 posit, Katanga, Democratic Republic of Congo: Quantitative Fluid Inclusion Analysis using Laser Ablation ICP-MS and Bulk Crush-Leach  
543 Methods. *Economic Geology*, 103(7):1459–1482, 11 2008. doi: 10.2113/gsecongeo.103.7.1459.

544 Hitzman, M. and Broughton, D. Discussion:“age of the zambian copperbelt” by sillitoe et al.(2017) mineralium deposita. *Mineralium De-  
545 posita*, 52(8):1273–1275, 2017.

546 Hitzman, M., Kirkham, R., Broughton, D., Thorson, J., and Selley, D. The Sediment-Hosted Stratiform Copper Ore System. In *One Hundredth*  
547 *Anniversary Volume*. Society of Economic Geologists, 2005. doi: 10.5382/AV100.19.

548 Hoffman, P. F., Abbot, D. S., Ashkenazy, Y., Benn, D. I., Brocks, J. J., Cohen, P. A., Cox, G. M., Creveling, J. R., Donnadieu, Y., Erwin, D. H.,  
549 Fairchild, I. J., Ferreira, D., Goodman, J. C., Halverson, G. P., Jansen, M. F., Hir, G. L., Love, G. D., Macdonald, F. A., Maloof, A. C., Partin,  
550 C. A., Ramstein, G., Rose, B. E. J., Rose, C. V., Sadler, P. M., Tziperman, E., Voigt, A., and Warren, S. G. Snowball Earth climate dynamics  
551 and Cryogenian geology-geobiology. *Science Advances*, 3(11):e1600983, 2017. doi: 10.1126/sciadv.1600983.

552 Hoggard, M. J., Czarnota, K., Richards, F. D., Huston, D. L., Jaques, A. L., and Ghelichkhan, S. Global distribution of sediment-hosted metals  
553 controlled by craton edge stability. *Nature Geoscience*, 13(7):504–510, jul 2020. doi: 10.1038/s41561-020-0593-2.

554 Holwell, D. A., Mitchell, C. L., Howe, G. A., Evans, D. M., Ward, L. A., and Friedman, R. The Munali Ni sulfide deposit, southern Zambia:  
555 A multi-stage, mafic-ultramafic, magmatic sulfide-magnetite-apatite-carbonate megabreccia. *Ore Geology Reviews*, 90:553–575, 2017.  
556 doi: <https://doi.org/10.1016/j.oregeorev.2017.02.034>.

557 Hu, X., Garzanti, E., Wang, J., Huang, W., An, W., and Webb, A. The timing of India-Asia collision onset – Facts, theories, controversies.  
558 *Earth-Science Reviews*, 160:264–299, 2016. doi: <https://doi.org/10.1016/j.earscirev.2016.07.014>.

559 Jackson, M., Warin, O., Woad, G., and Hudec, M. Neoproterozoic allochthonous salt tectonics during the Lufilian orogeny in the Katangan  
560 Copperbelt, central Africa. *Geological Society of America Bulletin - GEOL SOC AMER BULL*, 115:314–330, 03 2003. doi: 10.1130/0016-  
561 7606(2003)115<0314:NASTDT>2.0.CO;2.

562 John, T., Schenk, V., Haase, K., Scherer, E., and Tembo, F. Evidence for a Neoproterozoic ocean in south-central Africa from mid-  
563 oceanic-ridge-type geochemical signatures and pressure-temperature estimates of Zambian eclogites. *Geology*, 31(3):243, 2003.  
564 doi: 10.1130/0091-7613(2003)031<0243:EFANOI>2.0.CO;2.

565 John, T., Schenk, V., Mezger, K., and Tembo, F. Timing and PT Evolution of Whiteschist Metamorphism in the Lufilian Arc-Zambezi Belt  
566 Orogen (Zambia): Implications for the Assembly of Gondwana. *The Journal of Geology*, 112(1):71–90, jan 2004. doi: 10.1086/379693.

567 Johnson, S. P., Rivers, T., and Waele, B. D. A review of the Mesoproterozoic to early Palaeozoic magmatic and tectonothermal history of  
568 south-central Africa: implications for Rodinia and Gondwana. *Journal of the Geological Society*, 162(3):433–450, 2005. doi: 10.1144/0016-  
569 764904-028.

570 Johnson, S. P., Waele, B. D., and Liyungu, K. A. U-Pb sensitive high-resolution ion microprobe (SHRIMP) zircon geochronology of  
571 granitoid rocks in eastern Zambia: Terrane subdivision of the Mesoproterozoic Southern Irumide Belt. *Tectonics*, 25, 12 2006.  
572 doi: 10.1029/2006TC001977.

573 Johnson, S. P., De Waele, B., Evans, D., Banda, W., Tembo, F., Milton, J. A., and Tani, K. Geochronology of the Zambezi supracrustal sequence,  
574 southern Zambia: A record of neoproterozoic divergent processes along the southern Margin of the Congo Craton. *Journal of Geology*,

575 115(3):355–374, 2007. doi: 10.1086/512757.

576 Kampunzu, A. B., Tembo, F., Matheis, G., Kapenda, D., and Huntsman-Mapila, P. Geochemistry and Tectonic Setting of Mafic Igneous  
577 Units in the Neoproterozoic Katangan Basin, Central Africa: Implications for Rodinia Break-up. *Gondwana Research*, 3(2):125–153, 2000.  
578 doi: 10.1016/S1342-937X(05)70093-9.

579 Katongo, C., Koller, F., Kloetzli, U., Koeberl, C., Tembo, F., and Waele, B. D. Petrography, geochemistry, and geochronology of granitoid  
580 rocks in the Neoproterozoic-Paleozoic Lufilian-Zambezi belt, Zambia: Implications for tectonic setting and regional correlation. *Journal  
581 of African Earth Sciences*, 40(5):219–244, dec 2004. doi: 10.1016/j.jafrearsci.2004.12.007.

582 Kounoudis, R., Kendall, J. M., Ogden, C. S., Fishwick, S., Chifwepa, C., and Daly, M. C. The tectonic development of the Central African  
583 Plateau: evidence from shear-wave splitting. *Geophysical Journal International*, 239(3):1694–1708, oct 2024. doi: 10.1093/gji/ggae345.

584 Kuribara, Y., Tsunogae, T., Takamura, Y., and Tsutsumi, Y. Petrology, geochemistry, and zircon U-Pb geochronology of the Zam-  
585 bezi Belt in Zimbabwe: Implications for terrane assembly in southern Africa. *Geoscience Frontiers*, 10(6):2021–2044, 2019.  
586 doi: <https://doi.org/10.1016/j.gsf.2018.05.019>.

587 Lamont, T., McCarthy, W., Strachan, R., Roberts, N., Mackay-Champion, T., Bird, A., and Searle, M. Late Ordovician regional high-pressure  
588 metamorphism in Scotland: Caledonian metamorphic climax predated the closure of Iapetus. *EarthArXiv Preprint Server*, 3 2025.  
589 doi: 10.31223/X5W13Z.

590 Master, S. and Ndhlovu, N. M. *Geochemical, Microtextural, and Mineralogical Studies of the Samba Deposit in the Zambian Copperbelt Base-  
591 ment*, chapter 2, pages 37–55. American Geophysical Union (AGU), 2019. doi: <https://doi.org/10.1002/9781119290544.ch2>.

592 McCarthy, A., Chelle-Michou, C., Müntener, O., Arculus, R., and Blundy, J. Subduction initiation without magmatism: The case of the missing  
593 Alpine magmatic arc. *Geology*, 46(12):1059–1062, 10 2018. doi: 10.1130/G45366.1.

594 McCuaig, T. C. and Hronsky, J. M. A. The Mineral System Concept: The Key to Exploration Targeting. In *Building Exploration Capability for  
595 the 21st Century*. Society of Economic Geologists, 2014. doi: 10.5382/SP.18.08.

596 Milani, L., Lehmann, J., Naydenov, K. V., Saalmann, K., Kinnaird, J. A., Daly, J. S., Frei, D., and Sanz, A. L.-G. A-type magma-  
597 tism in a syn-collisional setting: The case of the Pan-African Hook Batholith in Central Zambia. *Lithos*, 216-217:48–72, feb 2015.  
598 doi: 10.1016/j.lithos.2014.11.029.

599 Milani, L., Lehmann, J., Naydenov, K. V., Saalmann, K., Nex, P. A., Kinnaird, J. A., Friedman, I. S., Woolrych, T., and Selley, D. Geology and  
600 mineralization of the Cu-rich Mumbwa district, a potential IOCG-type system at the eastern margin of the Pan-African Hook batholith,  
601 Zambia. *Journal of African Earth Sciences*, 158:103513, 2019. doi: <https://doi.org/10.1016/j.jafrearsci.2019.103513>.

602 Muchez, P., André-Mayer, A.-S., Desouky, H. A. E., and Reisberg, L. Diagenetic origin of the stratiform Cu–Co deposit at Kamoto in the Central  
603 African Copperbelt. *Mineralium Deposita*, 50:437–447, 4 2015. doi: 10.1007/s00126-015-0582-3.

604 Möller, C., Andersson, J., LUNDQVIST, I., and Hellström, F. Linking deformation, migmatite formation and zircon U–Pb geochronol-  
605 ogy in polymetamorphic orthogneisses, Sveconorwegian Province, Sweden. *Journal of Metamorphic Geology*, 25(7):727–750, 2007.  
606 doi: <https://doi.org/10.1111/j.1525-1314.2007.00726.x>.

607 Naydenov, K. V., Lehmann, J., Saalmann, K., Milani, L., Kinnaird, J. A., Charlesworth, G., Frei, D., and Rankin, W. New constraints on the Pan-  
608 African Orogeny in Central Zambia: A structural and geochronological study of the Hook Batholith and the Mwembeshi Zone. *Tectono-  
609 physics*, 637:80–105, 2014. doi: 10.1016/j.tecto.2014.09.010.

610 Naydenov, K. V., Lehmann, J., Saalmann, K., Milani, L., Poterai, J., Kinnaird, J. A., Charlesworth, G., and Kramers, J. D. The geology of the  
611 Matala Dome: an important piece of the Pan-African puzzle in Central Zambia. *International Journal of Earth Sciences*, 105(3):695–712,  
612 2016. doi: 10.1007/s00531-015-1222-y.

613 O'Brien, P. J. Eclogites and other high-pressure rocks in the Himalaya: a review. *Geological Society, London, Special Publications*, 483(1):  
614 183–213, 2019. doi: 10.1144/SP483.13.

615 Ogden, C. S., Kounoudis, R., Chifwepa, C., Kendall, M., Holwell, D., Fishwick, S., Nippes, S. E. J., Finch, L., Lane, V., and Daly, M. C. Crustal  
616 structure of the Central African Plateau from receiver function analysis. *Geophysical Journal International*, 241(2):1132–1144, 03 2025.  
617 doi: 10.1093/gji/ggaf083.

618 Padilla, A., Otarod, D., Deloach-Overton, S., Kemna, R., Freeman, P., Wolfe, E., Bird, L., Gulley, A., Trippi, M., Dicken, C., Hammarstrom, J.,  
619 and Brioche, A. Compilation of Geospatial Data (GIS) for the Mineral Industries and Related Infrastructure of Africa. Data release, U.S.  
620 Geological Survey, 2021. <https://doi.org/10.5066/P97EQWXP>.

621 Pankhurst, R. and Sutherland, D. Caledonian granites and diorites of Scotland and Ireland. 1982.

622 Parnell, J. and Boyce, A. J. Neoproterozoic copper cycling, and the rise of metazoans. *Scientific Reports*, 9:3638, 3 2019. doi: 10.1038/s41598-  
623 019-40484-y.

624 Perelló, J., Wilson, A., Wilton, J., and Creaser, R. A. Lufilian copper–gold mineralization in the Mkushi District, Zambia: regional metallogenic  
625 implications. *Mineralium Deposita*, 57(7):1089–1106, Oct. 2022. doi: 10.1007/s00126-022-01092-5.

626 Porada, H. and Berhorst, V. Towards a new understanding of the Neoproterozoic-Early Palaeozoic Lufilian and northern Zambezi Belts  
627 in Zambia and the Democratic Republic of Congo. *Journal of African Earth Sciences*, 30(3):727–771, 2000. doi: 10.1016/S0899-  
628 5362(00)00049-X.

629 Purkiss, M. Facies and sequence stratigraphy of the Katangan Basin in Zambia. *Journal of African Earth Sciences*, 227:105617, jul 2025.  
630 doi: 10.1016/j.jafrearsci.2025.105617.

631 Rainaud, C., Master, S., Armstrong, R., and Robb, L. Geochronology and nature of the Palaeoproterozoic basement in the Central African  
632 Copperbelt (Zambia and the Democratic Republic of Congo), with regional implications. *Journal of African Earth Sciences*, 42(1-5):1–31,  
633 jul 2005. doi: 10.1016/j.jafrearsci.2005.08.006.

634 Richards, J. P., Cumming, G. L., Krstic, D., Wagner, P. A., and Spooner, E. T. C. Pb isotope constraints on the age of sulfide ore deposition  
635 and U-Pb age of late uraninite veining at the Musoshi stratiform copper deposit, Central Africa copper belt, Zaire. *Economic Geology*, 83:  
636 724–741, 7 1988. doi: 10.2113/gsecongeo.83.4.724.

637 Ridgway, J. and Ramsay, C. A provisional metamorphic map of Zambia—explanatory notes. *Journal of African Earth Sciences* (1983), 5(5):  
638 441–446, 1986.

639 Saintilan, N. J., Selby, D., Creaser, R. A., and Dewaele, S. Sulphide Re-Os geochronology links orogenesis, salt and Cu-Co ores in the Central  
640 African Copperbelt. *Scientific Reports*, 8:14946, 10 2018. doi: 10.1038/s41598-018-33399-7.

641 Sakuwaha, K. G., Tsunogae, T., Banda, P., Changasha, C., Sikazwe, O. N., and Tsutsumi, Y. Neoproterozoic thermal events and crustal  
642 growth in the Zambezi Belt, Zambia: New insights from geothermobarometry, monazite dating, and detrital zircon geochronology of  
643 metapelites. *Lithos*, 424-425:106762, 2022. doi: <https://doi.org/10.1016/j.lithos.2022.106762>.

644 Sansjofre, P., Cartigny, P., Trindade, R. I., Nogueira, A. C., Agrinier, P., and Ader, M. Multiple sulfur isotope evidence for massive oceanic  
645 sulfate depletion in the aftermath of Snowball Earth. *Nature communications*, 7(1):12192, 2016.

646 Schaeffer, A. J. and Lebedev, S. Global shear speed structure of the upper mantle and transition zone. *Geophysical Journal International*,  
647 194(1):417–449, jul 2013. doi: 10.1093/gji/ggt095.

648 Scheller, E. L., Dickson, A. J., Canfield, D. E., Korte, C., Kristiansen, K. K., and Dahl, T. W. Ocean redox conditions between  
649 the snowballs – Geochemical constraints from Arena Formation, East Greenland. *Precambrian Research*, 319:173–186, 12 2018.  
650 doi: 10.1016/j.precamres.2017.12.009.

651 Searle, M., Cornish, S. B., Heard, A., Charles, J.-H., and Branch, J. Structure of the Northern Moine thrust zone, Loch Eriboll, Scottish  
652 Caledonides. *Tectonophysics*, 752:35–51, 2019. doi: <https://doi.org/10.1016/j.tecto.2018.12.016>.

653 Searle, M., Garber, J., Hacker, B., Htun, K., Gardiner, N., Waters, D., and Robb, L. Timing of Syenite-Charnockite Magma-  
654 tism and Ruby and Sapphire Metamorphism in the Mogok Valley Region, Myanmar. *Tectonics*, 39(3):e2019TC005998, 2020.  
655 doi: <https://doi.org/10.1029/2019TC005998>.

656 Searle, M. P. Tectonic evolution of the Caledonian orogeny in Scotland: a review based on the timing of magmatism, metamorphism and  
657 deformation. *Geological Magazine*, 159(1):124–152, 2022. doi: 10.1017/S0016756821000947.

658 Seifert, A. V., Žáček, V., Vrána, S., Pecina, V., Zachariáš, J., and Zwaan, J. C. Emerald mineralization in the Kafubu area, Zambia. *Bulletin of  
659 Geosciences*, 79:1–40, 2004.

660 Selley, D., Broughton, D., Scott, R., Hitzman, M., Bull, S., Large, R., McGoldrick, P., Croaker, M., Pollington, N., and Barra, F. A New Look at the  
661 Geology of the Zambian Copperbelt. In *One Hundredth Anniversary Volume*. Society of Economic Geologists, 2005. doi: 10.5382/AV100.29.

662 Selley, D., Scott, R., Emsbo, P., Koziy, L., Hitzman, M. W., Bull, S. W., Duffett, M., Sebagenzi, S., Halpin, J., and Broughton, D. W. Structural  
663 Configuration of the Central African Copperbelt: Roles of Evaporites in Structural Evolution, Basin Hydrology, and Ore Location. In *Metals,  
664 Minerals, and Society*. Society of Economic Geologists, 01 2018. doi: 10.5382/SP.21.07.

665 Sillitoe, R. H., Perelló, J., Creaser, R. A., Wilton, J., and Dawborn, T. Two Ages of Copper Mineralization in the Mwombezi Dome, Northwest-  
666 ern Zambia: Metallogenic Implications for the Central African Copperbelt. *Economic Geology*, 110(8):1917–1923, 12 2015. doi: 10.2113/e-  
667 congeo.110.8.1917.

668 Sillitoe, R. H., Perelló, J., Creaser, R. A., Wilton, J., Wilson, A. J., and Dawborn, T. Age of the Zambian Copperbelt. *Mineralium Deposita*, 52  
669 (8):1245–1268, dec 2017. doi: 10.1007/s00126-017-0726-8.

670 Simpson, J. G. The geology of the Mwembeshi River area. Explanation of Degree Sheet 1527, NE Quarter. Technical report, Geological  
671 Survey of Zambia, 1962.

672 St-Onge, M. R., Searle, M. P., and Wodicka, N. Trans-Hudson Orogen of North America and Himalaya-Karakoram-Tibetan Orogen of Asia:  
673 Structural and thermal characteristics of the lower and upper plates. *Tectonics*, 25(4), 2006. doi: <https://doi.org/10.1029/2005TC001907>.

674 Sun, Z., Lin, J., Qiu, N., Jian, Z., Wang, P., Pang, X., Zheng, J., and Zhu, B. The role of magmatism in the thinning and breakup of the  
675 South China Sea continental margin: Special Topic: The South China Sea Ocean Drilling. *National Science Review*, 6(5):871–876, 08 2019.  
676 doi: 10.1093/nsr/nwz116.

677 Taylor, C., Causey, J., Denning, P., Hammarstrom, J., Hayes, T., Horton, J., Kirschbaum, M., Parks, H., Wilson, A., Wintzer, N., and Zientek, M.  
678 Descriptive models, grade-tonnage relations, and databases for the assessment of sediment-hosted copper deposits—With emphasis on  
679 deposits in the Central African Copperbelt, Democratic Republic of the Congo and Zambia. *Scientific Investigations Report 2010-5090-J*,  
680 U.S. Geological Survey, 2013. <http://pubs.usgs.gov/sir/2010/5090/j/>. Includes data files.

681 Torrealday, H. Mineralization and alteration of the Kansanshi copper deposit, Zambia. Master’s thesis, Colorado School of Mines, 2000.

682 Turlin, F., Eglinger, A., Vanderhaeghe, O., André-Mayer, A.-S., Poujol, M., Mercadier, J., and Bartlett, R. Synmetamorphic Cu remo-  
683 bilization during the Pan-African orogeny: Microstructural, petrological and geochronological data on the kyanite-micaschists host-  
684 ing the Cu(-U) Lumwana deposit in the Western Zambian Copperbelt of the Lufilian belt. *Ore Geology Reviews*, 75:52–75, 2016.  
685 doi: <https://doi.org/10.1016/j.oregeorev.2015.11.022>.

686 van Gool, J. A. M., Rivers, T., and Calon, T. Grenville Front zone, Gagnon terrane, southwestern Labrador: Configuration of a midcrustal  
687 foreland fold-thrust belt. *Tectonics*, 27(1), 2008. doi: <https://doi.org/10.1029/2006TC002095>.

688 Villeneuve, M., Gärtner, A., Kalikone, C., and Wazi, N. Amalgamation in the Central African Shield (CAS) by the Kibaran

689 orogen: New hypothesis and implications for the Rodinia assembly. *Journal of African Earth Sciences*, 202:104936, 2023.  
690 doi: <https://doi.org/10.1016/j.jafrearsci.2023.104936>.

691 Vrána, S., Prasad, R., and Fediuková, E. Metamorphic kyanite eclogites in the lufilian arc of Zambia. *Contributions to Mineralogy and*  
692 *Petrology*, 51:139–160, 1975. doi: 10.1007/BF00403755.

693 Walraven, F. and Chabu, M. Pb-isotope constraints on base-metal mineralisation at Kipushi (Southeastern Zaïre). *Journal of African Earth*  
694 *Sciences*, 18(1):73–82, 1994. doi: [https://doi.org/10.1016/0899-5362\(94\)90055-8](https://doi.org/10.1016/0899-5362(94)90055-8).

695 Waters, D. J. Metamorphic constraints on the tectonic evolution of the High Himalaya in Nepal: the art of the possible. *Geological Society,*  
696 *London, Special Publications*, 483(1):325–375, 2019. doi: 10.1144/SP483-2018-187.

697 Weller, O. M., Mottram, C. M., St-Onge, M. R., Möller, C., Strachan, R., Rivers, T., and Copley, A. The metamorphic and magmatic record of  
698 collisional orogens. *Nature Reviews Earth Environment*, 2:781–799, 10 2021. doi: 10.1038/s43017-021-00218-z.

699 Wendorff, M. Evolution of Neoproterozoic–Lower Palaeozoic Lufilian arc, Central Africa: a new model based on syntectonic conglomerates.  
700 *Journal of the Geological Society*, 162(1):5–8, 2005. doi: 10.1144/0016-764904-085.

701 Yonkee, W. A. and Weil, A. B. Tectonic evolution of the Sevier and Laramide belts within the North American Cordillera orogenic system.  
702 *Earth-Science Reviews*, 150:531–593, 2015. doi: <https://doi.org/10.1016/j.earscirev.2015.08.001>.

703 Zhang, Y., Zhou, S., Wu, X., and Hu, Q. Genesis of the Samba Cu deposit of the Central African Copperbelt in Zambia: Constraints from  
704 geochemistry and geochronology. *GSA Bulletin*, 136(5-6):2343–2358, 10 2023. doi: 10.1130/B37146.1.